Dalton Transactions

ROYAL SOCIETY OF CHEMISTRY

PAPER

View Article Online
View Journal | View Issue

Cite this: *Dalton Trans.*, 2025, **54**, 4664

Dodecanuclear $[Ni^{II}_8Ln_4]$ clusters and rings of corner-sharing $\{Ni^{II}_2Ln_2\}$ cubanes (Ln = Dy, Gd, Y); magnetic and magnetothermal properties†

Thomais G. Tziotzi,[a] Eleftheria Agapaki,[b] Emmanouil K. Charkiolakis,[c] David Gracia,[c] Marc Ubach I. Cervera,[c] Scott J. Dalgarno,[d] Marco Evangelisti,*[c] Euan K. Brechin*[b] and Constantinos J. Milios*[a]

Received 21st January 2025,
Accepted 13th February 2025

DOI: 10.1039/d5dt00175g

rsc.li/dalton

The solvothermal reaction of $NiCl_2{\cdot}6H_2O$ with 1,3,5-tri(2-hydroxyethyl)-1,3,5-triazacyclohexane, LH_3, and $Ln(OAc)_3{\cdot}4H_2O$ in the presence of salicylaldehyde in MeOH leads to the formation of the dodecanuclear isostructural species $[Ni^{II}_8Ln_4(L')_8(OAc)_4(OH)_8(H_2O)_4]{\cdot}xH_2O$ (Ln = Dy, x = 6 (**1**); Gd, x = 24 (**2**); Y, x = 10 (**3**); L′ = the dianion of the Schiff-base resulting from the reaction of salicylaldehyde and ethanolamine). The metallic core of the clusters describes a ring of corner-sharing $\{Ni_2Ln_2\}$ cubanes assembled on a central, planar rectangular $\{Ln_4\}$ unit. Magnetization studies conducted on complexes **1–3** demonstrate the presence of dominant ferromagnetic exchange at low temperatures, which is largely attributed to the Ni···Ni interactions. The significant magnetocaloric effect observed in the Gd analogue has been assessed through heat capacity and magnetization measurements.

Introduction

The varied physical properties displayed by polymetallic complexes continues to attract the interest of the scientific community, since such species find application in various fields of science and technology, including luminescence, ferroelectricity, molecular imaging and applied bioinorganic chemistry.[1] Paramagnetic 3d–4f complexes displaying large spin ground-states resulting from ferro- or ferrimagnetic exchange are of particular interest in areas ranging from information storage to cryogenic refrigeration. For instance, certain 3d–4f clusters have been found to function as single-molecule magnets (SMMs), *i.e.* molecules that can retain their magnetization once magnetized in the absence of an external magnetic field.[2,3] A pertinent example is the recently reported metallacrown complex $\{Dy[15\text{-}MC_{Cu}\text{-}5]\}$, which displays the largest effective energy barrier (U = 625 cm^{-1}) for the re-orientation of the magnetization for any reported d–f SMM.[4] In addition, heterometallic 3d–4f clusters – particularly those based on Gd^{III} – have been employed as molecular coolants, since they can display an enhanced magnetocaloric effect at cryogenic temperatures.[5] A fine example being a $\{Ni_{21}Gd_{20}\}$ cage with an S = 91 spin ground-state and a low-field magnetic entropy of 14.1 J kg^{-1} K^{-1} for ΔB = 1 T at 1.1 K.[6]

We recently started exploring the use of the 1,3,5-tri(2-hydroxyethyl)-1,3,5-triazacyclohexane ligand, LH_3 (Scheme 1), in manganese chemistry, which led to the synthesis of a mixed-valent $\{Mn^{III}_{12}Mn^{II}_6\}$ wheel, a $\{Mn^{III}_{12}Mn^{II}_4\}$ double square wheel and a $\{Mn^{III}_{10}\}$ contorted wheel,[7] thus establishing the versatility of the LH_3 ligand towards the formation of polynuclear species. Given the tendency of the LH_3 ligand to promote the formation of mixed-valent species, we investigated its use in the M^{II}/Ln^{III} (M = Ni, Co) reaction system. Herein we report the synthesis and characterisation of three

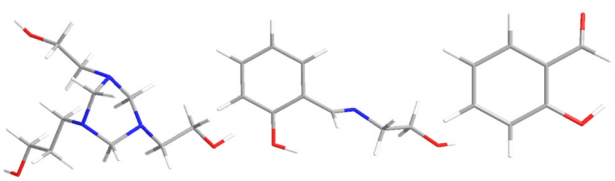

Scheme 1 The ligands discussed in the text; LH_3 (left), $L'H_2$ (middle) and salicylaldehyde (right). Colour code: C = grey, N = blue, O = red, H = white

[a]*Department of Chemistry, The University of Crete, Voutes, 71003 Herakleion, Greece. E-mail: komil@uoc.gr*
[b]*EaStCHEM School of Chemistry, The University of Edinburgh, David Brewster Road, Edinburgh, Scotland, EH9 3FJ, UK. E-mail: E.Brechin@ed.ac.uk*
[c]*Instituto de Nanociencia y Materiales de Aragón (INMA), CSIC – Universidad de Zaragoza, 50009 Zaragoza, Spain. E-mail: evange@unizar.es*
[d]*Institute of Chemical Sciences, Heriot-Watt University, Riccarton, Edinburgh, Scotland, EH14 4AS, UK*

†Electronic supplementary information (ESI) available: PXRD patterns (Fig. S1), EDS spectra (Fig. S2), SHAPE calculations (Table S1). CCDC 2410260–2410262. For ESI and crystallographic data in CIF or other electronic format see DOI: https://doi.org/10.1039/d5dt00175g

dodecanuclear heterometallic $[Ni^{II}_8Ln^{III}_4(L')_8(OAc)_4(OH)_8(H_2O)_4]\cdot xH_2O$ (Ln = Dy, x = 6 (**1**); Gd, x = 24 (**2**); Y, x = 10 (**3**)) complexes formed upon the decomposition of the LH_3 ligand under the solvothermal conditions and the *in situ* formation of the dianion of the Schiff-base between salicylaldehyde and ethanolamine, L′.

Experimental

General methods

All chemicals were obtained from commercial suppliers (Sigma-Aldrich) and were used without further purification/treatment.

Synthesis

LH_3 was prepared as previously described.[8]

$[Ni^{II}_8Dy_4(OH)_8(OAc)_4(L')_8(H_2O)_4]\cdot 6H_2O$ (1·6H$_2$O). $NiCl_2\cdot 6H_2O$ (118.5 mg, 0.5 mmol), $Dy(OAc)_3\cdot 4H_2O$ (206 mg, 0.5 mmol), salicylaldehyde (61 mg, 0.5 mmol) and LH_3 (103 mg, 0.5 mmol) were added to MeOH (18 ml), in the presence of NEt_3 (0.15 ml, 1.0 mmol) and the resulting mixture transferred to a Teflon-lined autoclave (23 ml) and kept at 120 °C for 12 hours. After slow cooling to room temperature at a rate of 10 °C h^{-1}, olive-green rod-like crystals of **1** were obtained in ∼35% yield, collected by filtration, washed with Et_2O and dried under vacuum. Elemental analysis (%) calcd for $C_{80}H_{104}Dy_4N_8Ni_8O_{38}$ (**1**·2H$_2$O): C 33.07, H 3.61, N 3.86; found: C 32.94, H 3.43, N 3.81.

$[Ni^{II}_8Gd_4(OH)_8(OAc)_4(L')_8(H_2O)_4]\cdot 24H_2O$ (**2**·24H$_2$O) was prepared in a similar manner to **1** using $Gd(OAc)_3\cdot 4H_2O$ instead of $Dy(OAc)_3\cdot 4H_2O$. Elemental analysis (%) calcd for $C_{80}H_{110}Gd_4N_8Ni_8O_{41}$ (**2**·5H$_2$O): C 32.70, H 3.77, N 3.81; found: C 32.59, H 3.61, N 3.72.

$[Ni^{II}_8Y_4(OH)_8(OAc)_4(L')_8(H_2O)_4]\cdot 10H_2O$ (3·10H$_2$O). $Ni(OAc)_2\cdot 4H_2O$ (124 mg, 0.5 mmol), YCl_3 (98 mg, 0.5 mmol), salicylaldehyde (61 mg, 0.5 mmol) and LH_3 (103 mg, 0.5 mmol) were added to MeOH (18 ml), in the presence of NEt_3 (0.15 ml, 1.0 mmol) and the resulting mixture was transferred to a Teflon-lined autoclave (23 ml). The autoclave was kept at 120 °C for 12 hours, and after slow cooling to room temperature (10 °C h^{-1}), dark-green rod-like crystals of **3** were obtained in ∼30% yield and collected by filtration and dried under vacuum. Elemental analysis (%) calcd for $C_{80}H_{108}N_8Ni_8O_{40}Y_4$ (**3**·4H$_2$O): C 36.30, H 4.11, N 4.25; found: C 36.21, H 3.97, N 4.14.

Crystallography

Using Olex2,[9] single crystal X-ray structures were solved with the SHELXT[10] structure solution program using Intrinsic Phasing and refined with the SHELXL[11] refinement package using least squares minimisation. **Crystal data for 1 (CCDC 2410260†):** $C_{80}H_{112}Dy_4N_8Ni_8O_{42}$ (M = 2977.45 g mol^{-1}), monoclinic, space group $C2/c$, a = 20.9513(16) Å, b = 19.9583(16) Å, c = 25.322(2) Å, β = 101.165(4)°, V = 10 388.1(14) Å^3, Z = 4, T = 195(2) K, Bruker Apex II diffractometer, μ(MoKα) = 4.331 mm^{-1}, D_{calc} = 1.835 g cm^{-3}, 126 728 reflections measured (4.622° ≤ 2Θ ≤ 56.668°), 12 917 unique (R_{int} = 0.0578, R_{sigma} = 0.0304) which were used in all calculations. The final R_1 was 0.0402 ($I > 2\sigma(I)$) and wR_2 was 0.1076 (all data). **Crystal data for 2 (CCDC 2410261†):** $C_{80}H_{148}Gd_4N_8Ni_8O_{60}$ (M = 3280.74 g mol^{-1}), monoclinic, space group $C2/c$, a = 20.9663(10) Å, b = 20.0465(9), c = 26.2609(13) Å, V = 10 830.3(9) Å^3, Z = 4, T = 210(2) K, Bruker Apex II diffractometer, μ(MoKα) = 3.874 mm^{-1}, D_{calc} = 2.012 g cm^{-3}, 314 922 reflections measured (4.36° ≤ 2Θ ≤ 58.306°), 14 593 unique (R_{int} = 0.0573, R_{sigma} = 0.0195) which were used in all calculations. The final R_1 was 0.0514 ($I > 2\sigma(I)$) and wR_2 was 0.1225 (all data). **Crystal data for 3 (CCDC 2410262†):** $C_{80}H_{120}N_8Ni_8O_{46}Y_4$ (M = 2755.15 g mol^{-1}), monoclinic, space group $C2/c$, a = 20.9054(7) Å, b = 19.9035(6) c = 26.4714(8) Å, V = 10 798.1(6) Å^3, Z = 4, T = 220(2) K, Bruker Apex II diffractometer, μ(MoKα) = 3.571 mm^{-1}, D_{calc} = 1.695 g cm^{-3}, 85 906 reflections measured (4.522° ≤ 2Θ ≤ 57.514°), 13 988 unique (R_{int} = 0.0857, R_{sigma} = 0.0701) which were used in all calculations. The final R_1 was 0.0528 ($I > 2\sigma(I)$) and wR_2 was 0.1348 (all data).

Magnetometry

Magnetization data were collected on MPMS-XL and MPMS3 SQUID magnetometers equipped with 5 and 7 T magnets, respectively. Diamagnetic corrections were applied using Pascal's constants.

Heat capacity

Heat capacity measurements were carried out on a PPMS equipped with a 9 T magnet and a ^{3}He cryostat, using a thin pressed pellet (*ca.* 1 mg) of a polycrystalline sample of **2**, thermalized by *ca.* 0.2 mg of Apiezon N grease, whose contribution was subtracted using a phenomenological expression.

Powder XRD measurements

Powder XRD measurements were collected on freshly prepared samples of **1–3** on a PANanalytical X'Pert Pro MPD diffractometer.

Infra-red spectroscopy

FTIR-ATR (Fourier-transform infrared-attenuated total reflectance) spectra were recorded on a PerkinElmer FTIR Spectrum BX spectrometer.

Energy-dispersive X-ray spectroscopy

EDS measurements were performed on a JEOL Scanning Electron Microscope.

Results and discussion

The initial system investigated was the simple synthetic triad of $Ni^{II}/Dy^{III}/LH_3$ in the absence of any co-ligands. However, after many experiments in which all synthetic parameters were varied (*i.e.* reaction times, presence/absence of base, bench/

solvothermal conditions, metal salts and metal : ligand ratios) no crystalline material was obtained. We employed salicylaldehyde as a co-ligand in the reaction system, since it is well-known that it can serve both as a chelate ligand (blocking polymerisation and the formation of aggregates) as well as a bridging ligand *via* the deprotonation of the hydroxyl group. The 1 : 1 : 1 : 1 solvothermal reaction of LH_3 with $NiCl_2{\cdot}6H_2O$, $Dy(OAc)_3{\cdot}4H_2O$ and salicylaldehyde in basic methanolic solution produced olive-green crystals of $[Ni^{II}_8Dy^{III}_4(L')_8(OAc)_4(OH)_8(H_2O)_4]{\cdot}6H_2O$ (**1**·$6H_2O$) in good yields. The crystal structure of the complex (*vide infra*) revealed the presence of the dianion of the Schiff-base ligand that forms from the reaction between salicylaldehyde and ethanolamine, the latter originating from the dissociation of the LH_3 ligand to its components under the high-temperature and high-pressure conditions of the autoclave. Repeating the same reaction under ambient conditions led to the formation of a green solution, which yielded a crude oil upon standing. The gadolinium and yttrium analogues of complex **1** were formed following analogous synthetic routes (in the case of the yttrium analogue YCl_3 was used as the yttrium salt) and are isostructural with **1**. Despite the fact that the Schiff-base ligand produced *in situ*, L′H_2, has been extensively employed for the formation of metallic clusters,[12] this is the first time that the formation of such large 3d–4f species is observed.

Since complexes **1–3** are isostructural, we limit discussion to the crystal structure of **1**. Complex **1** crystallises in the monoclinic space group *C*2/*c* (Fig. 1). Its metallic core describes a central, planar rectangular $\{Dy_4\}$ unit of dimension ~3.9 × 3.7 Å, serving as a base for the assembly of four $\{Ni_2Dy_2(OH)_2(O_R)_2\}$ cubes in a circular fashion, with each cube sharing two Dy corners (Dy1, Dy2 and symmetry equivalents, s.e.) with two neighboring cubes. All cubes are distorted with: (i) edge dimensions ranging from ~2.06 to 2.37 Å, (ii) Dy–O(H)–Dy angles in the ~109.7–112.8° range, (iii) Ni–O_R–Ni angles of ~97°, (iv) Ni–$O_{R/H}$–Dy angles in the ~91.0–104.5° range and (v) Ni···Ni distances in the ~3.10–3.15 Å range.

All eight L′ ligands are found in an $\eta^3{:}\eta^1{:}\eta^1{:}\mu_3$ coordination mode, bridging two Ni and one Dy centres within each cube, while eight μ_3-OH^- bridges (O3, O9, O12, O14, and s.e., BVS values = 0.77–0.88) complete the formation of the cubes. Neighbouring cubes are linked to each other *via* one $\eta^2{:}\eta^1{:}\mu_3$ acetate, bridging two Ni and one Dy centres. All eight Ni ions are six-coordinate with a $\{O_5N\}$ coordination sphere, adopting octahedral geometry. The only exceptions to this are Ni1 and Ni3 which adopt severely distorted octahedral geometries as evidenced by: (i) the presence of a large bonding distance (Ni1–O4 = 2.43 Å and Ni3–O18′ = 2.38 Å) and (ii) the deviations of the O2′–Ni1–O4 and O7–Ni3–O18′ angles of ~136° and 135°, respectively, from the theoretical value of 180° (Fig. 2). The coordination environment of the 4f ions is completed by the presence of a terminal H_2O molecule, with all Dy^{III} cations being eight-coordinate and square-antiprismatic (SHAPE analysis, Table S1†).[13]

In the extended structure, molecules of **1** pack in a "brickwork" like manner, forming sheets in the *ab* plane, with the water solvate molecules occupying the void space between the clusters (Fig. 3). There exists an intricate inter- and intramolecular hydrogen-bonded network mediated by the eight water molecules.

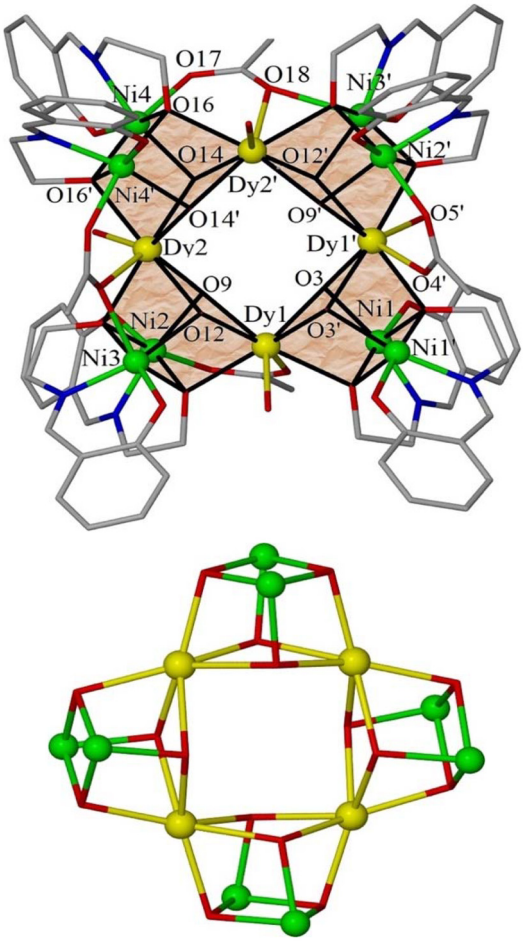

Fig. 1 The crystal structure of **1** (top) highlighting the assembly of the four $\{Ni_2Dy_2\}$ cubes, and its metal-oxygen core viewed along the *c* axis (bottom). Colour code: Dy^{III} = yellow, Ni^{II} = green, O = red, N = blue, C = grey. H-atoms and solvate water molecules have been omitted for clarity.

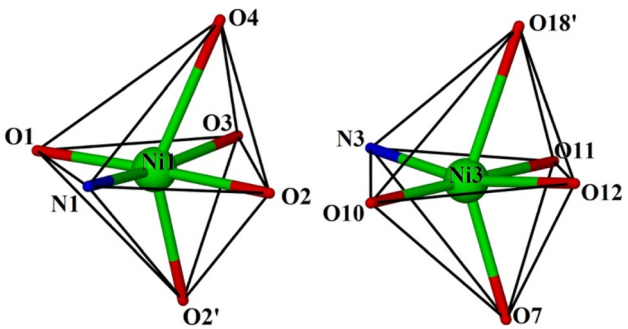

Fig. 2 The severely distorted octahedral geometry for Ni1 and Ni3 (and s.e.). Colour code: Ni^{II} = green, O = red, N = blue.

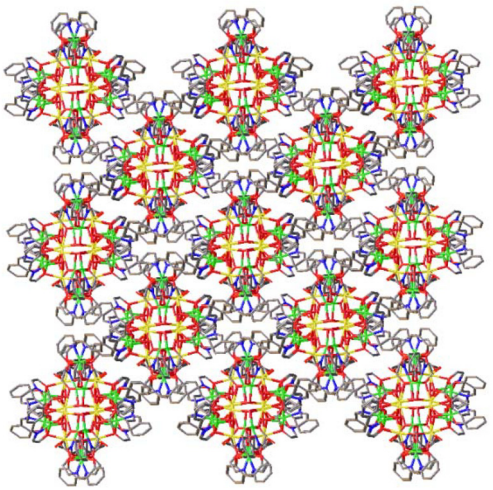

Fig. 3 The crystal packing of **1** in the *ab* plane. Solvate molecules and H-atoms are omitted. Colour code: Dy^{III} = yellow, Ni^{II} = green, O = red, N = blue.

Magnetic properties

The direct current molar magnetic susceptibility, χ_M, of freshly prepared polycrystalline samples of **1–3** were measured in an applied field, B, of 0.1 T, over the 2–300 K temperature, T, range. The purity of all samples was established by means of PXRD comparison with the simulated data from the single-crystal structure (Fig. S1†), as well as from EDS measurements (Fig. S2†). The experimental results are presented in the form of the $\chi_M T$ product *vs.* T in Fig. 4a.

The experimental room-temperature $\chi_M T$ values of 62.3 cm^3 K mol^{-1} for **1**, 39.1 cm^3 K mol^{-1} for **2** and 9.3 cm^3 K mol^{-1} for **3**, respectively, are close to the theoretical values expected for eight independent Ni^{II} ions (g_{Ni} = 2.0) and four Dy^{III} ions (s = 5/2, L = 5, J = 15/2, g_J = 4/3) of 64.7 cm^3 K mol^{-1} (for **1**), eight independent Ni^{II} ions (g_{Ni} = 2.0) and four Gd^{III} ions (g_{Gd} = 2.0) of 39.5 cm^3 K mol^{-1} (for **2**), and eight independent Ni^{II} ions (g_{Ni} = 2.0) of 8.0 cm^3 K mol^{-1} (for **3**). For **1**, the $\chi_M T$ value decreases slowly upon cooling from room temperature down to ~60 K, below which it steeply increases reaching 69.9 cm^3 K mol^{-1} at T = 2 K, indicating the presence of ferromagnetic exchange interactions. For **2**, $\chi_M T$ slightly increases upon

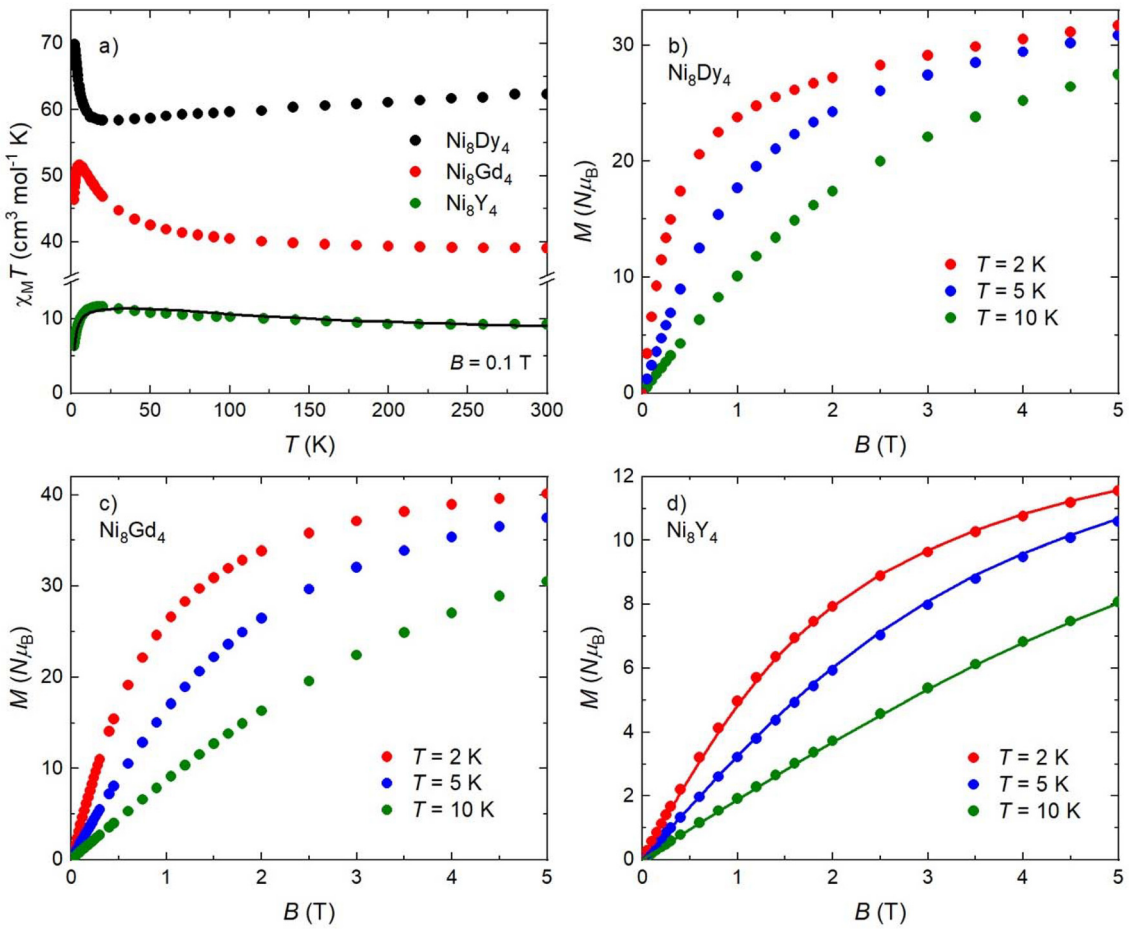

Fig. 4 Temperature dependence of the $\chi_M T$ product for complexes **1–3** (a), collected under an applied magnetic field of B = 0.1 T, and isothermal molar magnetization M *versus* applied magnetic field, for **1** (b) **2** (c) and **3** (d), collected for T = 2, 5 and 10 K. Symbols are experimental data, while lines are fits for **3** (see main text).

cooling down to ~70 K, while upon further cooling it increases rapidly to reach the maximum value of 51.6 cm^3 K mol^{-1} at T = 5.5 K, before it drops to 46.4 cm^3 K mol^{-1} at the lowest temperature of 2 K, suggesting dominant ferromagnetic interactions. The abrupt drop at the lowest T may be attributed to ZFS and/or intermolecular interactions. For **3**, the $\chi_M T$ product decreases slowly upon cooling until ~50 K, below which it slightly increases reaching a maximum value of 11.6 cm^3 K mol^{-1} at T = 18 K, denoting dominant ferromagnetic exchange. Upon further cooling, it decreases steeply reaching 6.3 cm^3 K mol^{-1} at T = 2 K. This is attributed to the presence of antiferromagnetic exchange and/or crystal field effects. For **1**, ac susceptibility measurements (not shown here) in the temperature range 2–30 K, at zero-applied field, reveal no evidence of slow relaxation of the magnetic moment. Low-temperature variable-temperature and variable-field magnetization, M, data were measured in the temperature range 2–7 K, in magnetic fields up to 5.0 T for complexes **1** and **3**, and up to 7.0 T for complex **2** (Fig. 4b–d and S3†). At the lowest temperature and highest field measured, M reaches a value of 31.7μ_B and 11.6μ_B for **1** and **3**, respectively, while for the Gd analogue **2** a value of 40.1μ_B is obtained.

The magnetic properties of **3** can be well accounted for by a simple theoretical model of dimeric $\{Ni_2\}$ units, $\mathcal{H} = -2J_{Ni}\sum \vec{s}\cdot\vec{s} + D_{Ni}s_z^2 + g_{Ni}\mu_B Bs$. The best fit of the $\chi_M T$ *vs.* T (Fig. 4a) and M *vs.* B (Fig. 4d) data affords D_{Ni}/k_B = 11.5 K, g_{Ni} = 2.0 and J_{Ni}/k_B = 29.4 K, denoting a relatively strong ferromagnetic Ni···Ni exchange interaction. For **1** and **2**, the diagonalization of the corresponding Hamiltonians and the calculation of observables are not feasible due to the large dimensions of the associated Hilbert spaces.

Magnetothermal properties and MCE

The magnetocaloric effect (MCE), that is, the change of magnetic entropy ΔS_m and adiabatic temperature ΔT_{ad} in response to a change of the applied magnetic field ΔB, can be significantly large in selected molecular clusters. Given that Gd^{III} is the typical ion of choice due to the large s = 7/2 and negligible anisotropy, we pursued magnetocaloric studies of complex **2**. The heat capacity c_p of a sample of **2** was measured over the 0.3–30 K temperature range in selected applied fields B = 0, 1, 3 and 7 T (Fig. 5). A strong field dependence is particularly visible at temperatures below ~10 K, while the nonmagnetic lattice contribution tends to dominate at the larger temperatures. The analysis that is systematically carried out for this class of molecular materials, consists of fitting the high-field, low-temperature c_p data to Debye's law, *i.e.*, $c_{latt} = a \times T^3$, where the coefficient a typically has values of the order of 10^{-2} K^{-3}.[14,15] However, the experimental c_p data of **2** are approximately one order of magnitude larger than the expected c_{latt} below 1 K (Fig. 5), making characterization unfeasible.

Exchange interactions involving Gd^{III} ions lose dominance against the Zeeman term of the Hamiltonian when increasing the magnetic field. The model proposed to evaluate c_p collected at the higher field values neglects all exchange interactions but Ni···Ni from the dimeric $\{Ni\}_2$ units, which we assume to be the same as in **3**. The Schottky curves were calculated for four dimeric $\{Ni\}_2$ units and four free Gd^{III} ions per molecular unit, shown in Fig. 5 as the dashed and dotted curves, respectively. The sum of both contributions leads to the solid line that fits the experimental c_p data at B = 7 T. Exchange correlations involving Gd^{III} ions become domi-

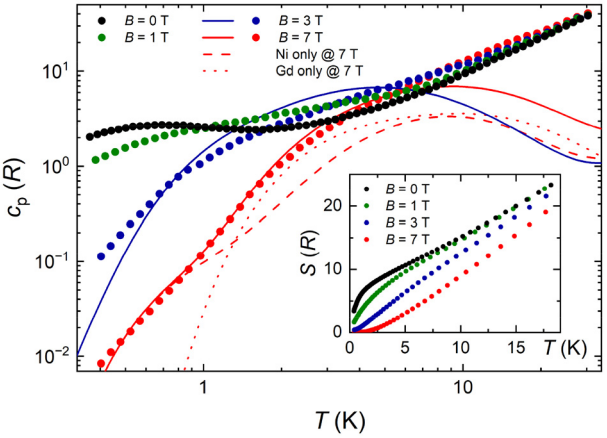

Fig. 5 Molar heat capacity c_p and entropy S (inset) *versus* temperature for selected applied field values for **2**. Symbols are experimental data, while lines are theoretical simulations (see main text).

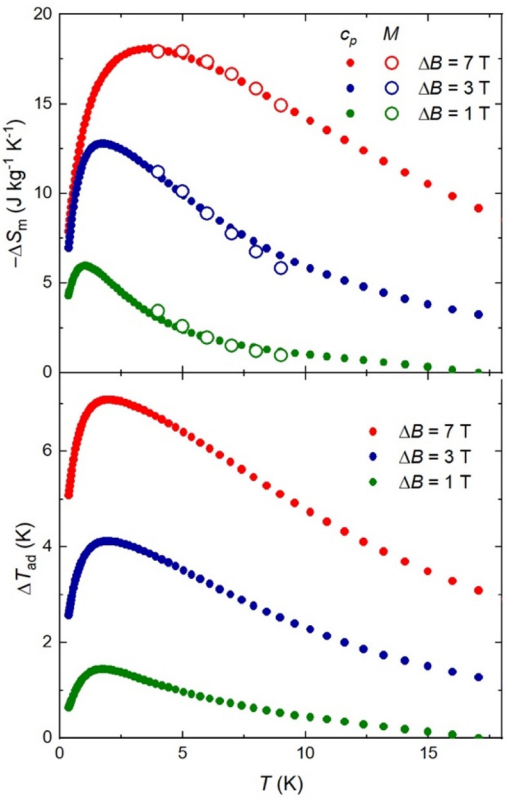

Fig. 6 Magnetic entropy change ΔS_m (top) and adiabatic temperature change ΔT_{ad} (bottom) *versus* temperature for **2**, calculated from magnetization (empty symbols) and heat capacity (filled symbols) data.

Table 1 Magnetocaloric properties of representative Ni/Gd clusters

Formula	$-\Delta S_m$ J kg^{-1} K^{-1}	T (K)	ΔB (T)	Ref.
$[Ni_6Gd_6(OH)_2(O_3PCH_2Ph)_6(O_2C^tBu)_{16}(MeCO_2H)_2]\cdot 4MeCN$	26.5	3.0	7	16
$[Gd_{36}Ni_{12}(CH_3COO)_{18}(\mu_3\text{-}OH)_{84}(\mu_4\text{-}O)_6(H_2O)_{54}(NO_3)Cl_2](NO_3)_6Cl_9\cdot 30H_2O$	36.3	3.0	7	17
$[Gd_{42}Ni_{10}(\mu_3\text{-}OH)_{68}(CO_3)_{12}(CH_3COO)_{30}(H_2O)_{70}]\cdot(ClO_4)_{24}\cdot 80H_2O$	38.2	2.0	7	18
$[Ni^{II}{}_8Gd_4(OH)_8(OAc)_4(L')_8(H_2O)_4]\cdot 24H_2O$	18.1	3.7	7	This work
$[Ni_2Gd(L)_6](NO_3)$	13.7	4.0	7	19
$[NiGd(HL)_2(NO_3)_3]$	5.7	7.0	7	20
$[Gd_2Ni_2(NO_3)_6(H_2O)_{1.5}(CH_3CN)_2(L)_2]\cdot CH_3CN$	18.5	3.0	5	21
$[Ni(H_2O)_6][Gd(oda)_3]\cdot 3H_2O$	31.6	2.0	9	22
$[Ni_{64}Gd_{96}(\mu_3\text{-}OH)_{156}(IDA)_{66}(DMPA)_{12}(CH_3COO)_{48}(NO_3)_{24}(H_2O)_{64}]Cl_{24}\cdot 35CH_3OH\cdot 120H_2O$	42.8	3.0	7	23
$[Ni_4Gd_4(\mu_2\text{-}OH)_2(\mu_3\text{-}OH)_4(\mu\text{-}OOCCH_3)_8(LH_2)_4]\cdot(OH)_2\cdot H_2O$	22.6	3.0	5	24
$[Na_2Gd_{78}Ni_{64}(IDA)_{58}(OAc)_2(SiO_4)_6(Cl)_4(\mu_2\text{-}OH)_4(\mu_4\text{-}O)_4(\mu_3\text{-}O)_{38}(\mu_3\text{-}OH)_{126}(H_2O)_{82}]\cdot(Cl)_4(H_2O)_{37}$	40.6	3.0	7	25
$[Ni_{36}Gd_{102}(OH)_{132}(mmt)_{18}(dmpa)_{18}(H_2dmpa)_{24}(CH_3COO)_{84}(SO_4)_{18}(NO_3)_{18}(H_2O)_{30}]\cdot Br_6(NO_3)_6\cdot(H_2O)_{130}\cdot(CH_3OH)_{60}$	41.3	2.0	7	26
$[Ni_5Gd_8(\mu_3\text{-}OH)_7(\mu\text{-}OH_2)(O_3P\text{-}^tBu)_6(O_2C\text{-}^tBu)_{15}(MeCN)]$	30.6	3.0	7	27
$[Gd_{152}Ni_{14}Cl_{24}(CO_3)_{42}(OAc)_{48}(H_2O)_{138}(OH)_{308}]\cdot Cl_{20}\cdot(H_2HEIDA)_{10}\cdot 20H_2O$	52.7	3.5	7	28
$[Gd_{22}Ni_{22}(DTA)_{21}(SO_4)_4(OH)_{48}(OCH_3)_4](NO_3)_6\cdot(H_2O)_{50}$	46.0	2.0	7	29
$\{[Gd_2Ni(L)(C_2O_4)_2(H_2O)_2]\cdot H_2O\}_n$	38.0	2.0	7	30

nant for fields lower than 3 T, breaking the agreement between the experiment and model.

Next, we calculate the temperature dependence of the entropy, S (inset of Fig. 5), for any B value from the experimental c_p, using

$$S(T,B) = \int_0^T \frac{c_p(T',B)}{T'}\mathrm{d}T'.$$

The zero-field applied entropy increases sharply on increasing T at low temperatures, reaching values of $7R$ = 16.3 J kg^{-1} K^{-1} near 1–2 K. The available magnetic entropy content, *i.e.*, $S_m = [8 \times \ln(2 \times 1 + 1) + 4 \times \ln(2 \times 3.5 + 1)]R = 17.1R$ = 39.7 J kg^{-1} K^{-1}, is not attained at low temperatures due to the relatively strong Ni···Ni interactions. At high temperatures, all experimental curves at different fields tend to overlap because of the nonmagnetic lattice contribution.

To evaluate the MCE, ΔS_m and ΔT_{ad} are obtained as differences between entropy curves, for magnetic field changes $\Delta B = B - 0$. ΔS_m is also calculated from the magnetization curves of Fig. 4 using the Maxwell relation,

$$\Delta S_m(T,\Delta B) = \int_0^B \left[\frac{\partial M}{\partial T}\right]_B \mathrm{d}B.$$

The ΔS_m results from both calculations overlap, proving the validity of our approach (Fig. 6). The magnetic entropy change reaches 18.1 J kg^{-1} K^{-1}, which corresponds to ~46% of the available entropy at 3.7 K for the largest applied field of 7 T. The adiabatic temperature change shows a maximum of 7.1 K at T = 2 K for ΔB = 7 T. Complex **2** joins a growing family of heterometallic Ni–Gd clusters displaying a relatively large $-\Delta S_m$ value (Table 1).

Conclusions

In conclusion, in this work we report three isostructural dodecanuclear $\{Ni_8Ln_4\}$ (Ln = Dy, Gd and Y) complexes, upon the *in situ* formation of the dianionic form of the Schiff-base ligand resulting from the reaction of salicylaldehyde and ethanolamine. All three clusters feature an aesthetically pleasing ring-like assembly of four $\{Ni_2Ln_2(OH)_2(O_R)_2\}$ cubes arranged in a circular fashion around a planar $\{Ln_4\}$ rectangle. The study of the magnetic properties revealed dominant ferromagnetic interactions in the Y analogue (complex **3**), while the Gd analogue (complex **2**) displays a significant magnetocaloric effect.

Author contributions

TGT synthesized and characterized the complexes. SJD solved the single-crystal XRD data. EA, EKC, DG and ME measured the magnetic/heat capacity data and analysed the MCE parameters. MU and ME simulated the magnetic/heat capacity data. EKB and CJM conceived the idea. All authors contributed to writing the manuscript.

Data availability

Crystallographic data for compounds **1–3** have been deposited at the CCDC under numbers 2410260–2410262.† Further data supporting this manuscript have been included as part of the ESI.† All data presented in this article can be retrieved from DIGITAL.CSIC at **https://doi.org/10.20350/digitalCSIC/17066**.

Conflicts of interest

There are no conflicts to declare.

Acknowledgements

This work has received support from EU (MSCA-DN MolCal, 101119865), MICIU/AEI/10.13039/501100011033/ and ERDF/EU

(PID2021-124734OB-C21, CEX2023-001286-S), Gobierno de Aragón (E11-23R, E12-23R). CJM and TGT would like to thank the National Recovery and Resilience Plan Greece 2.0 (Award Number TAEDR-0535821), funded by the European Union – NextGenerationEU.

References

1 See for example: J. Long, J. Rouquette, J.-M. Thibaud, R. A. S. Ferreira, L. D. Carlos, B. Donnadieu, V. Vieru, L. F. Chibotaru, L. Konczewicz, J. Haines, Y. Guari and J. Larionova, *Angew. Chem., Int. Ed.*, 2015, **54**, 2236–2240; A. J. Amoroso and S. A. J. Pope, *Chem. Soc. Rev.*, 2015, **44**, 4723–4742; C. Zhang, C. Chen, H. Dong, J. R. Shen, H. Dau and J. Zhao, *Science*, 2015, **348**, 690–693.

2 For representative reviews on SMMs see: D. Gatteschi and R. Sessoli, *Angew. Chem., Int. Ed.*, 2003, **42**, 268–297; G. Christou, D. Gatteschi, D. N. Hendrickson and R. Sessoli, *MRS Bull.*, 2000, **25**, 66–71; C. J. Milios and R. E. P. Winpenny, *Struct. Bonding*, 2015, **164**, 1–109; L. Sorace, C. Benelli and D. Gatteschi, *Chem. Soc. Rev.*, 2011, **40**, 3092–3104; X.-Y. Wang, C. Avendañoa and K. R. Dunbar, *Chem. Soc. Rev.*, 2011, **40**, 3213–3238; R. A. Layfield, *Organometallics*, 2014, **33**, 1084–1099; L. K. Thompson and L. N. Dawe, *Coord. Chem. Rev.*, 2015, **289**, 13–31; S. Demir, I.-R. Jeon, J. R. Long and T. D. Harris, *Coord. Chem. Rev.*, 2015, **289**, 149–176; P. Happ, C. Plenk and E. Rentschler, *Coord. Chem. Rev.*, 2015, **289**, 238–260; G. A. Craig and M. Murrie, *Chem. Soc. Rev.*, 2015, **44**, 2135–2147; A. Chakraborty, J. Goura, P. Kalita, A. Swain, G. Rajaraman and V. Chandrasekhar, *Dalton Trans.*, 2018, **47**, 8841–8864; A. Zabala-Lekuona, J. M. Seco and E. Colacio, *Coord. Chem. Rev.*, 2021, **441**, 213984.

3 F.-S. Guo, B. M. Day, Y.-C. Chen, M.-L. Tong, A. Mansikkamäki and R. A. Layfield, *Science*, 2018, **362**, 1400–1403; C. A. Gould, K. R. McClain, D. Reta, J. G. C. Kragskow, D. A. Marchiori, E. Lachman, E.-S. Choi, J. G. Analytis, R. D. Britt, N. F. Chilton, B. G. Harvey and J. R. Long, *Science*, 2022, **375**, 198–202.

4 J. Wang, Q.-W. Li, S.-G. Wu, Y.-C. Chen, R.-C. Wan, G.-Z. Huang, Y. Liu, J.-L. Liu, D. Reta, M. J. Giansiracusa, Z.-X. Wang, N. F. Chilton and M.-L. Tong, *Angew. Chem., Int. Ed.*, 2020, **60**, 5299–5306.

5 See for example: J. W. Sharples, D. Collison, E. J. L. McInnes, J. Schnack, E. Palacios and M. Evangelisti, *Nat. Commun.*, 2014, **5**, 5321; G. Lorusso, O. Roubeau and M. Evangelisti, *Angew. Chem., Int. Ed.*, 2016, **55**, 3360–3363; G. Lorusso, J. W. Sharples, E. Palacios, O. Roubeau, E. K. Brechin, R. Sessoli, A. Rossin, F. Tuna, E. J. L. McInnes, D. Collison and M. Evangelisti, *Adv. Mater.*, 2013, **25**, 4653–4656; G. Lorusso, M. Jenkins, P. González-Monje, A. Arauzo, J. Sesé, D. Ruiz-Molina, O. Roubeau and M. Evangelisti, *Adv. Mater.*, 2013, **25**, 2984–2988; M. Evangelisti, Molecule-Based Magnetic Coolers: Measurement, Design and Application, in *Molecular Magnets: Physics and Applications*, ed. J. Bartolomé, F. Luis and J. F. Fernández, Springer Verlag, Berlin Heidelberg, 2014, pp. 365–387.

6 W.-P. Chen, J. Singleton, L. Qin, A. Camón, L. Engelhardt, F. Luis, R. E. P. Winpenny and Y.-Z. Zheng, *Nat. Commun.*, 2018, **9**, 2107.

7 T. G. Tziotzi, M. Coletta, M. Gray, C. L. Campbell, S. J. Dalgarno, G. Lorusso, M. Evangelisti, E. K. Brechin and C. J. Milios, *Inorg. Chem. Front.*, 2021, **8**, 1804–1809; M. Coletta, T. G. Tziotzi, M. Gray, G. S. Nichol, M. K. Singh, C. J. Milios and E. K. Brechin, *Chem. Commun.*, 2021, **57**, 4122–4125.

8 M. V. Baker, D. H. Brown, B. W. Skelton and A. H. White, *J. Chem. Soc., Dalton Trans.*, 1999, 1483–1490.

9 O. V. Dolomanov, L. J. Bourhis, R. J. Gildea, J. A. K. Howard and H. Puschmann, OLEX2: A Complete Structure Solution, Refinement and Analysis Program, *J. Appl. Crystallogr.*, 2009, **42**, 339.

10 G. M. Sheldrick, SHELXT – Integrated space-group and crystal-structure determination, *Acta Crystallogr., Sect. A: Found. Adv.*, 2015, **71**, 3.

11 G. M. Sheldrick, Crystal structure refinement with SHELXL, *Acta Crystallogr., Sect. C: Struct. Chem.*, 2015, **71**, 3.

12 See for example: C. Boskovic, A. Sieber, G. Chaboussant, H. U. Gudel, J. Ensling, W. Wernsdorfer, A. Neels, G. Labat, H. Stoeckli-Evans and S. Janssen, *Inorg. Chem.*, 2004, **43**, 5053; C. Boskovic, R. Bircher, P. L. W. Tregenna-Piggott, H. U. Gudel, C. Paulsen, W. Wernsdorfer, A.-L. Barra, E. Khatsko, A. Neels and H. Stoeckli-Evans, *J. Am. Chem. Soc.*, 2003, **125**, 14046; A. K. Jami, S. P. Behera, S. Mondal and V. Baskar, *Inorg. Chem. Commun.*, 2022, **143**, 109784; D. Basak, J. van Leusen, T. Gupta, P. Kögerler and D. Ray, *Dalton Trans.*, 2020, **49**, 7576; C. Boskovic, H. U. Gudel, G. Labat, A. Neels, W. Wernsdorfer, B. Moubaraki and K. S. Murray, *Inorg. Chem.*, 2005, **44**, 3181; D. Basak, E. R. Martí, M. Murrie, I. Nemec and D. Ray, *Dalton Trans.*, 2021, **50**, 9574; O. Stetsiuk, N. Plyuta, N. Avarvari, E. Goreshnik, V. Kokozay, S. Petrusenko and A. Ozarowski, *Cryst. Growth Des.*, 2020, **20**, 1491; I. C. Lazzarini, L. Carrella, E. Rentschler and P. Albores, *Polyhedron*, 2012, **31**, 779; Y.-G. Li, L. Lecren, W. Wernsdorfer and R. Clérac, *Inorg. Chem. Commun.*, 2004, **7**, 1281; H. Oshio, N. Hoshino, T. Ito and M. Nakano, *J. Am. Chem. Soc.*, 2004, **126**, 8805; N. Hoshino, T. Ito, M. Nihei and H. Oshio, *Inorg. Chem. Commun.*, 2003, **6**, 377; D. S. Nesterov, E. N. Chygorin, V. N. Kokozay, V. V. Bon, R. Boča, Y. N. Kozlov, L. S. Shul'pina, J. Jezierska, A. Ozarowski, A. J. L. Pombeiro and G. B. Shul'pin, *Inorg. Chem.*, 2012, **51**, 9110.

13 M. Llunell, D. Casanova, J. Girera, P. Alemany and S. Alvarez, *SHAPE, version 2.0*, Barcelona, Spain, 2010.

14 T. G. Tziotzi, D. Gracia, S. J. Dalgarno, J. Schnack, M. Evangelisti, E. K. Brechin and C. J. Milios, *J. Am. Chem. Soc.*, 2023, **145**, 7743–7747.

15 E. Agapaki, E. K. Charkiolakis, G. S. Nichol, D. Gracia, M. Evangelisti and E. K. Brechin, *Front. Chem.*, 2024, **12**, 1494609.

16 Y. Zheng, M. Evangelisti and R. E. P. Winpenny, *Angew. Chem., Int. Ed.*, 2011, **50**, 3692–3695.
17 J. Peng, Q. Zhang, X. Kong, Y. Ren, L. Long, R. Huang, L. Zheng and Z. Zheng, *Angew. Chem., Int. Ed.*, 2011, **50**, 10649–10652.
18 J.-B. Peng, Q.-C. Zhang, X.-J. Kong, Y.-Z. Zheng, Y.-P. Ren, L.-S. Long, R.-B. Huang, L.-S. Zheng and Z. Zheng, *J. Am. Chem. Soc.*, 2012, **134**, 3314–3317.
19 A. Upadhyay, N. Komatireddy, A. Ghirri, F. Tuna, S. K. Langley, A. K. Srivastava, E. C. Sañudo, B. Moubaraki, K. S. Murray, E. J. L. McInnes, M. Affronte and M. Shanmugam, *Dalton Trans.*, 2014, **43**, 259–266.
20 N. Ahmed, C. Das, S. Vaidya, A. K. Srivastava, S. K. Langley, K. S. Murray and M. Shanmugam, *Dalton Trans.*, 2014, **43**, 17375–17384.
21 C. Meseguer, S. Titos-Padilla, M. M. Hänninen, R. Navarrete, A. J. Mota, M. Evangelisti, J. Ruiz and E. Colacio, *Inorg. Chem.*, 2014, **53**, 12092–12099.
22 J. Qiu, L. Wang, Y. Chen, Z. Zhang, Q. Li and M. Tong, *Chem. – Eur. J.*, 2016, **22**, 802–808.
23 W. Chen, P. Liao, Y. Yu, Z. Zheng, X. Chen and Y. Zheng, *Angew. Chem., Int. Ed.*, 2016, **55**, 9375–9379.
24 P. Kalita, J. Goura, J. M. Herrera, E. Colacio and V. Chandrasekhar, *ACS Omega*, 2018, **3**, 5202–5211.
25 Q. Lin, J. Li, X. Luo, C. Cui, Y. Song and Y. Xu, *Inorg. Chem.*, 2018, **57**, 4799–4802.
26 W.-P. Chen, P.-Q. Liao, P.-B. Jin, L. Zhang, B.-K. Ling, S.-C. Wang, Y.-T. Chan, X.-M. Chen and Y.-Z. Zheng, *J. Am. Chem. Soc.*, 2020, **142**, 4663–4670.
27 Y. Zhai, W. Chen, M. Evangelisti, Z. Fu and Y. Zheng, *Aggregate*, 2024, **5**, e520.
28 N. Xu, W. Chen, Y.-S. Ding and Z. Zheng, *J. Am. Chem. Soc.*, 2024, **146**, 9506–9511.
29 Z. Lu, C. Duan and J. Wang, *J. Mol. Struct.*, 2024, **1312**, 138622.
30 Q. Wang, L. Xu, J. Wang, Y. Yu, X. Bai, C. Jiang, Q. Chen and Y. Xu, *Dalton Trans.*, 2025, **54**, 2930–2936.